International Journal of Modern Agriculture, Volume 10, No.2, 2021
ISSN: 2305-7246

Investigations to reveal the nature of interactions of Bovine hemoglobin with Curcumin nanoparticle using spectroscopic techniques

S.Bakkialakshmi[*1], S.Chithra[2]

[1,2] Department of Physics, Annamalai university, Annamalainagar, Tamilnadu, India

Abstract

Curcumin is a major bioactive compound found in the Curcuma longa rhizome. The Curcumin Nanoparticles System (Cur-NS) was developed through the process of ionic gelation and defined by the study of particle size, FTIR and SEM. This research aims to explore the relationship of ultraviolet-visible (UV-Vis) absorption, fluorescence, time-resolved fluorescence, synchronous fluorescence and molecular docking methods between the Curcumin nanoparticle system (Cur-NS) and Bovine hemoglobin (BHb). The findings showed that, through the increase in Cur-NS concentration, the fluorescence intensity of BHb was reduced. There was an estimate of binding constants and the number of binding sites. The binding distance to the tryptophan residues of BHb between Cur-NS was 2.23 nm. Results of UV-Vis spectra, synchronous fluorescence spectra, have shown that Cur-NS can alter the confirmation of BHb, which may influence the physiological functions of hemoglobin. In addition, the findings of molecular docking revealed that the experimental fluorescence results were in accordance with the results obtained by molecular docking.

Introduction

The principal yellow bioactive portion of turmeric (Curcuma longa), a permanent plant of the ginger group (Zingiberaceae), inhabitant to South Asia's Tropical [1], is turcumin, a 1,7-bi(4-hydroxy-3-methoxyphenyl)-1,6 heptadiene-3,5-dione. It is used widely as a seasoning, preservative and colouring agent for food. With a wide variety of biological uses, it is a non-toxic, highly promising natural antioxidant compound. Due to its possible medicinal significance, curcumin has recently attracted intense attention [2-13].

Curcumin has two aromatic rings bound by α, β-unsaturated-β-diketone, with phenolic OH groups. Ketoenol tautomerism is present in solutions to the β-diketone structure [14]. In the visible region, curcumin absorbs and provides fluorescence with a low quantum yield. The characteristics of pollution are heavily dependent on the polarity of the environment [14].

Fig.1. shows structure of curcumin. Continuous investigations and clinical trials give sufficient confirmation that this natural phenolic product has various pharmacological activities. The compound is sometimes referred to as a chemo-preventive agent against cancer in addition to its powerful antioxidant, antibiotic, antimicrobial/antiviral and anti-inflammatory properties [15,16,17]. The intrinsic fluorescence of BHb, particularly around Tryptophan (Trp) residues, is susceptible to its microenvironment, like most proteins. Any aspects, such as protein confirmational transition, denaturation, biomolecular binding etc. [18], it can affect the fluorescence intensity of the protein. The interaction process between BHb and Cur-NS was analysed here using various spectroscopic techniques that are effective and sensitive, such as fluorescence, UV-Vis and FTIR.

This paper discusses the binding mechanism of Cur-NS to bovine hemoglobin (BHb) under pretend physiological condition by fluorescence, UV-Vis absorption and molecular docking. The energy transfer is recorded between BHb and Cur-NS. Furthermore, the confirmation changes of BHb arising in the existence of Cur-NS have been studied by using time-resolved and synchronous fluorescence approaches. The report attempts to explain the binding mechanisms of bovine hemoglobin to food colourants and offers inklings to the biochemical consequences and roles of food colourants in the body.

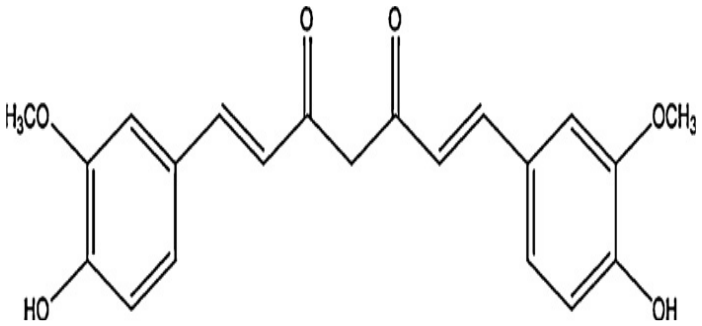

Fig.1 Structure of curcumin.

2. Experimental

2.1. Materials

Bovine Hemoglobin and curcumin were purchased from Sigma–Aldrich (Bangalore). Low molecular weight Chitosan (CS) and sodium tripolyphosphate (TPP) were purchased from Sisco research laboratory (Chennai).

2.2. Preparation of Cur-NS

For the formulation of Cur-NS as [19,20] in which Chitosan polycation groups are associated with polyanionic TPP, modified ionic gelation was performed. The ethanol solution of curcumin was poured into the solution of chitosan (0.6 %, w/v), collected at room temperature by softening CS in dilute acetic acid (1%, v/v). TPP, dissolved at 5 mg/ml (w/v) in de-ionized water, was immediately applied dropwise to the emulsion [20]. Thus, the nanoparticles that were magnetically stirred (100 rpm) at room temperature were produced instantaneously upon the dropwise addition of TPP solution. The CS/TPP ratio for the construction of the nanoparticle system in the formulations was held at 3:1 (w/w). The resulting colloidal assembly system was incessantly mixed for 30 minutes, i.e., the formulation of the nanoparticle system, and the outcomes collected were extracted by centrifugation for 15 minutes at 2000 rpm, washed with distilled deionized water to extract ethanol.

2.3. Characterization of Curcumin nanoparticles system (Cur-NS)

By the particle size analyzer, the particle size was determined (Micrometrics CPE-11 Nano plus). Furthermore, the scanning electron microscope is used to determine the morphological characteristics of the nanoparticles (JEOL-JSM-IT 200). An X-Ray Diffractometer evaluated the XRD for Cur-NS (BRUCKER D8 Advance). The Cur-NS and Curcumin powder FTIR spectra were analyzed by FTIR spectroscopy (AGILENT CARY 630 FTIR Spectrometer).

2.4. Spectroscopic instruments details

Absorption spectral studies were recorded using UV/Visible spectrophotometer (SHIMADZU 1800 PC UV/VISIBLE SPECTROPHOTOMETER). Steady state fluorescence measurements were performed on Shimadzu RF-5301 PC (Shimadzu Corporation, Kyoto, Japan). Fluorescence decay measurements were recorded using Hariba-Jobin Yvon [spex-sf B-III] spectrofluorimeter. FT-Raman spectra were recorded utilizing BRUKER RFS-27 STAND alone FT-Raman Spectrometer.

2.5. Molecular docking Study

In edict to calculate the interaction approaches between Cur-NS and BHb, the AutoDock [21] software was used. To predict the probable conformation of Cur-NS that binds to the protein, the Lamarckian genetic algorithm (LGA) executed in AutoDock was pragmatic. The BHb crystal structure was taken from the protein data bank of Brookhaven (http://www.rcsb.org/pdb) (PDB ID:1G09). The results have been analysed by Autodock and PyMOL software.

2.6. Antibacterial activity using Agar Well Diffusion Method

In the agar well diffusion process, screening of the antimicrobial activity of mucus extracts was performed using Muller Hinton agar (MHA) medium for antibacterial activity. From a 24-hour culture colony on a nutrient broth substrate, bacterial and fungal inoculums were prepared. To attain a final concentration of between 104 and 106 CFU/mL for the bacteria, the inoculum was calibrated with the McFarland density. In the Whatmann AA filter paper, 50µg of each extract was imbibed and applied to the test media which had subsequently been inoculated with each test strain. Bacteria plates are incubated at 37^0C. After 24 hours of incubation, inhibition zones were analyzed [22].

Results and discussion

3.1. Characterization of Curcumin nanoparticles (Cur-NS)

3.1.1 UV-Visible spectroscopy

UV-Visible spectrometry is the most common method for determining the size and composition of nanoparticles. These nanoparticles are generally susceptible to colloids due to the intense peak of absorption caused by the excitation of the surface plasmon. The UV/Visible Spectrophotometer SHIMADZU 1800 PC UV/Visible Spectrophotometer was used to do the analysis. A small aliquot of the reaction mixture was taken, with a wavelength range of 200 nm to 800 nm. As shown in Fig.1, the UV-Visible results indicate that Cur-NS has a typical absorption peak at 271.

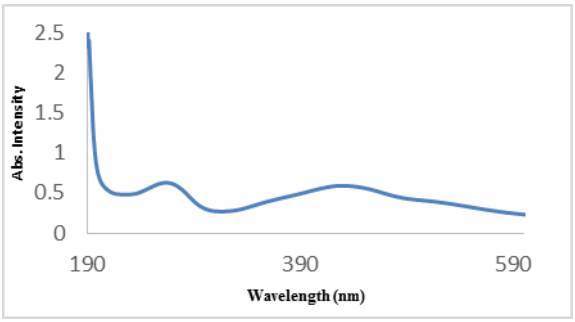

Fig.1 UV/Vis absorption spectra of Cur-NS

3.1.2. Particles size Analyser

The particle size was determined using a particle size analyzer. The experiment was implemented at a temperature of 25^0C with water as the solvent. As a result of the study, the average particle size of the Cur-NS formulation is 277.2 nm (Fig.3) of particles in the nanometer size range, which is as predicted. Colloid nanoparticles have many advantages, including the fact that their nano-size makes them much more stable against sediment. The particle size calculation yielded a polydispersibility index of 0.349. The polydispersibility index specifies the particle size distribution found in nanoparticle preparation; the lower the polydispersibility index, the more uniform the particle sizes are, and the particle properties are changed if there is a noticeable variation in size between larger and smaller particles. The simpler it is to settle the particles, the more contaminants there are [23].

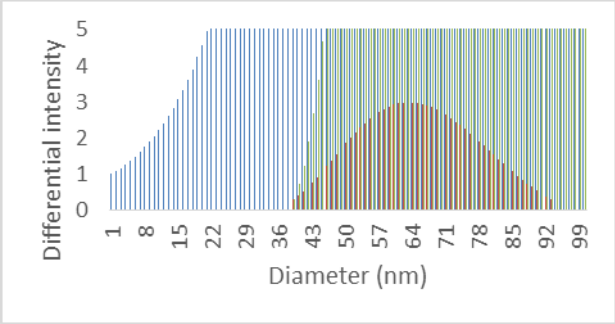

Fig.3 Particle size analysis of Cur-NS

3.1.3. Scanning Electron Microscopy (SEM)

The morphology of nanoparticles on the surface was studied using SEM microscopy. At different magnifications, SEM images were obtained. A well, decidedly dispersed beam of electron is screened terminated a reedy sample, and the electrons paging over the specimen are collected on a detector placed underneath the specimen, resulting in the preferred intense pasture images. SEM will allow us to have a more accurate estimate of nanoparticle size distribution. Fig. 4 shows an irregular nanoparticle structure with a diameter ranging from 50 to 450 nm. The emitted electrons are guided through a standard detector using an electron multiplier, which is a gold sheet.

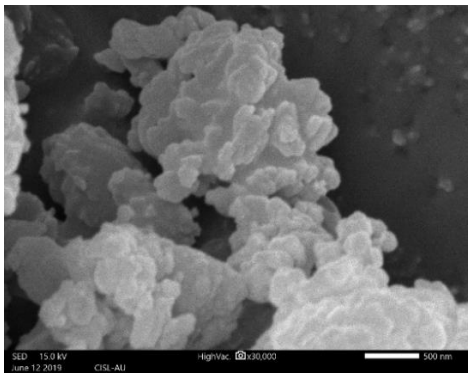

Fig.4 SEM image of Curcumin nanoparticles

3.1.4. XRD Analysis

The crystalline state of the samples was determined using an x-ray diffractometer. The appearance of many separate peaks at 2(38.03), showing that the Cur-NS was of a fine crystalline type, was shown by the XRD patterns at flow rates (8 and 10 ml / min) and the assay, as shown in Fig.5.

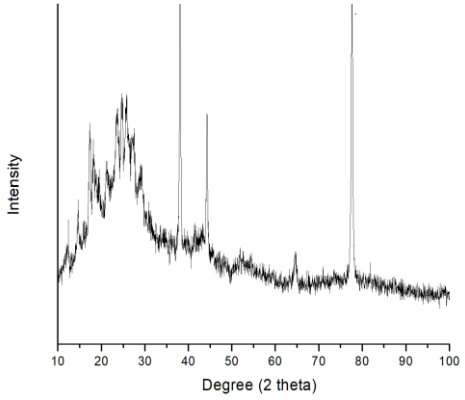

Fig.5 X-Ray diffraction pattern of Curcumin nanoparticles

3.1.5. FTIR studies

The structural modification of Cur food colorant after it was converted into nanoparticles was investigated using FTIR measurements. When the FTIR spectra of Cur-NS and Cur are compared, most of the peaks obtained by Cur are repeated in the FTIR spectrum of Cur-NS, and the spectrum of Cur-NS does not change significantly (Fig. 6). In the case of curcumin, spectrum bands appeared at 3453 cm^{-1} for the phenolic OH, 2848 cm^{-1} for the CH bond, 1624 cm^{-1} for the C=O bond of the conjugated ketone, 1458 cm^{-1} for the CH_2 bond, 1426 cm^{-1} for the stretching of the C=C bond of the aromatic ring, 1376 cm^{-1} for the CH_3 bond, and 1024 cm^{-1} for the stretching of the C-O-C bond [24].

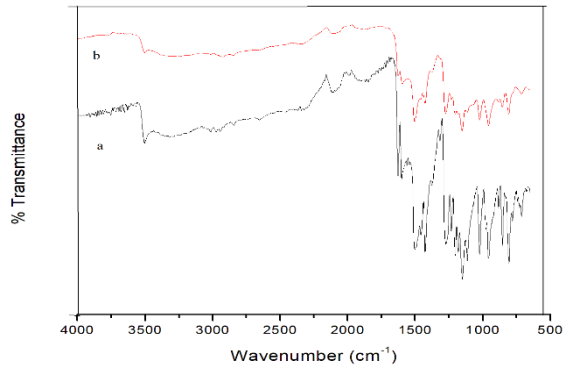

Fig.6 FTIR spectra of a) Curcumin b) Curcumin nanoparticles

3.2. UV-Vis spectroscopic study for BHb with Curcumin nanoparticles

At 200, 280, and 405 nm, the absorption spectrum of BHb showed three peaks in Fig. 7. Trp and tyrosine (Tyr) residues have a phenyl group that appears as a band at 280 nm, while the porphyrin-Soret band has a sharp peak at 405 nm. The heme group is trapped in a hydrophobic pocket created by the protein's backbone after proper folding, forming this band [25,26]. The peptide bond induces an absorption peak at 200 nm, which represents the α-helix structure's microenvironment in BHb [27]. The absorbances of peaks at 200 and 280 nm increased consistently as Cur-NS was added to the BHb solution, meaning that the Cur-NS induced the squander of the BHb minimal erection and facilitated the disclosure of aromatic ring amino acids in the intramural hydrophobic region. A blue shift from 280 to 255 nm was seen in the peak at 280 nm. Due to the dispersal of peptide chains, Cur-NS readily combines into the hydrophobic pocket of BHb. The amino acids in BHb are eventually revealed. The heme groups are liberated from the hydrophobic cavity of BHb, which intensifies its intrinsic absorption peak [28].

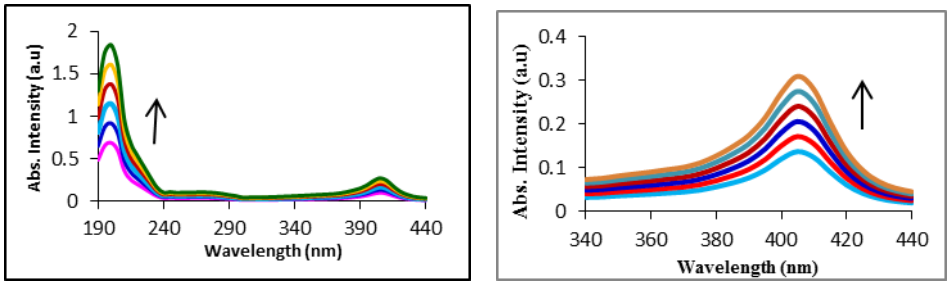

Fig.7 (a) UV-Vis absorption spectra of BHb with different concentrations Cur-NS (mol L^{-1}) (1) 0.0, (2) 0.2, (3) 0.4, (4) 0.6, (5) 0.8, (6) 1.0. (b) The 405 nm band is highlighted.

3.3. Steady state fluorescence

Fluorescence quenching is described as a reduction in the quantum yield of fluorescence from a fluorophore due to a combination of molecular interactions with the quencher molecule, such as excited-state reactions, energy conversion, molecule rearrangement, collision quenching and ground state complex formation. Simultaneously, due to its sensitivity and ease of use, it is an effective instrument for researching the interactions of substances with proteins.

Fluorescence quenching can be divided into two categories: dynamic and static. A quenching collision, also known as dynamic quenching, happens when fluorophores collide with a quencher. Dynamic quenching has to do with temperature. Higher temperature is estimated to result in a higher coefficient of diffusion, as well as higher bimolecular quenching constants [29]. The presence of a ground state complex between the fluorophores and the quencher induces static quenching [30]. For the quenching process research, it's necessary to consider the quenching technique and process. The quenching mechanism is explained using binding constants. Fig.8 shows the influence of Cur-NS on BHb fluorescence intensity. As the concentration of Cur-NS increased, the fluorescence intensity of BHb decreased gradually, without changing the emission maximum or peak form, meaning that Cur-NS interacted with BHb. To validate the quenching process, the Stern–Volmer equation [31] was used to analyse the fluorescence quenching data:

$$F_0/F = 1+K_q\,\tau_0\,[Q] = 1+K_{sv}\,[Q] \qquad (1)$$

The fluorescence intensities are F_0 and F, respectively, before and after the quencher is inserted. K_{SV} is the Stern–Volmer quenching constant, and [Q] is the quencher concentration. The K_{SV} values obtained from the Stern–Volmer plot in Fig.9 were used to define the static quenching of BHb fluorescence in the binding mechanism.

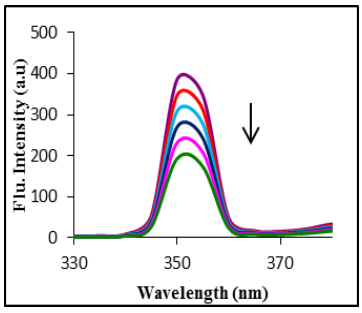

Fig.8 Steady–state fluorescence spectra of BHb with different concentrations of Cur- NS (mol L^{-1}) (1) 0.0, (2) 0.2, (3) 0.4, (4) 0.6, (5) 0.8, (6) 1.0.

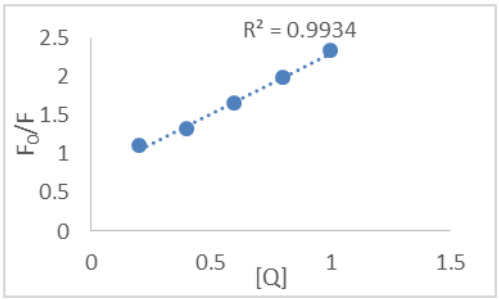

Fig. 9 Stern-Volmer plot for the quenching of BHb by Cur-NS concentrations

3.4. Fluorescence Lifetime Study

Fluorescence quenching including time-resolved fluorescence analysis, according to Lakowicz's theory, can effectively differentiate among static and dynamic processes [32]. Dynamic quenching is characterized by major changes in fluorescence lifetime values, although static quenching is characterized by equal fluorescence lifetime values [32]. As seen in Fig.10, time-resolved fluorescence lifetime measurements for BHb were

performed in the absence and presence of Cur-NS. The fluorescence lifetime values and related amplitudes of free and complexed BHb were calculated using time-resolved fluorescence decay curves. Here, τ = fluorescence lifetime and α = relative amplitude. For free BHb, the fluorescence lifetime values were τ_1= 2.43 ns and τ_2= 7.4 ns. The average fluorescence lifetime values after the addition of Cur-NS were determined to be τ_1= 1.7 ns and τ_2= 7.01 ns, respectively. Specific components were not allocated because the Trp residues have multi exponential decays [33]. Instead, the overall fluorescence lifetime was used to obtain qualitative insights. The fluorescence lifetime of free BHb was 3.03 ns on average, but it was decreased to 1.84 ns in the presence of Cur-NS. The fluorescence lifetime of free BHb was almost unchanged in the presence of Cur-NS. This finding confirmed that the quenching process is mostly unchanged and is caused by BHb and Cur-NS complexation.

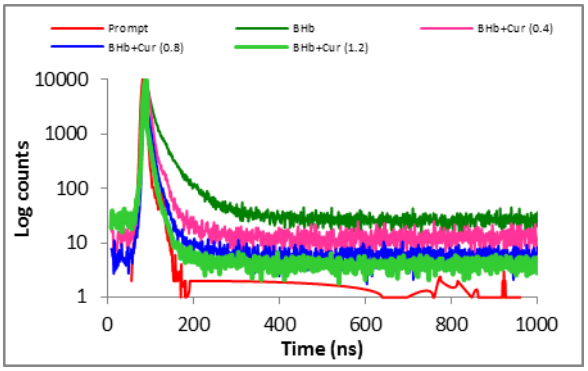

Fig.10 Time – resolved fluorescence spectra of BHb with different concentrations of Cur-NS (mol L^{-1}) (1)0.0, (2)0.4, (3)0.8, (4)1.2.

3.5. Binding constants and number of binding sites

Fluorescence quenching techniques can be used to determine the binding constant (K_a) and the number of binding sites (n) dependent on the interaction of Cur-NS with BHb. Under the presumption that proteins have independent binding sites, the values of K_a and n can be determined [34].

$$\text{Log } (F_O - F)/F = \log K_a + n \log [Q] \qquad (2)$$

The fluorescence intensities of the protein with and without quencher are F and F_0, respectively, and [Q] is the initial quencher concentration. Fig.11 depicts the results of fluorescence quenching studies, while Table 1 mentions the computed results. In 1:1M concentration ratios, the results suggested that BHb had only one equivalent binding sites with Cur-NS, implying that a complex formed between Cur-NS and BHb. In general, if K_a is greater than 10,000, the binding is strong [35]. The K_a value of 1.07 x10^5 can be found in Table1, showing that Cur-NS and BHb had a strong binding interaction. As a result, the Cur-NS could quickly interact with Hb in the human body, affecting its biological function.

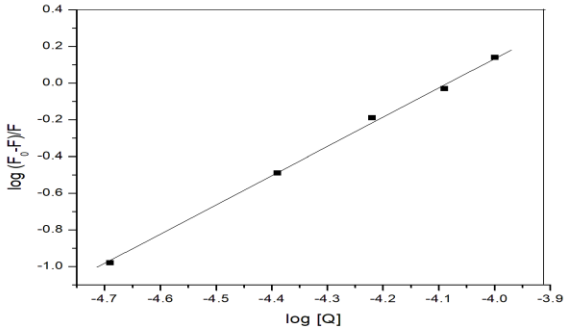

Fig.11 The plot of log (F_0-F)/F versus log (Q)

Table 1. Stern–Volmer (K_{SV}) and bimolecular quenching rate constant (K_q),

binding constant (K_a) and binding site (n) of BHb with Cur-NS

Quenchers	**K_{SV} x 10^5 (L mol^{-1})**	**K_q x 10^8 (L $mol^{-1}S^{-1}$)**	**K_a x10^5 (L mol^{-1})**	**n**
Curcumin - NP	1.15	3.78	1.07	1.25

3.6. Conformation investigation

The calculated synchronous fluorescence spectra of BHb with addition of Cur-NS are provided here to obtain more information around the confirmational shift of BHb caused by Cur-NS.

The synchronous fluorescence spectroscopy method, first proposed by Lloyd [36] in1971, involves scanning the excitation and emission monochromators at the same time while keeping a fixed wavelength interval between them. The synchronous fluorescence provides the characteristics information of the Tyr or Trp residues as described by the Miller [37] if the D-value (Δλ) is stable at 15 and 60 nm between wavelengths of excitation and emission. Fig. 12a and 12b display the influence of Cur-NS on BHb synchronous fluorescence spectra. During the interaction of BHb with Cur-NS, the maximum emission wavelength of Tyr and Trp residues almost stayed unchanged, showing that the polarity around Tyr and Trp residues is still maintained [38]. The slight loss of α-helical secondary structure caused by Cur-NS have no effect on the polarity and hydrophobicity around the Tyr and Trp residues in protein [39].

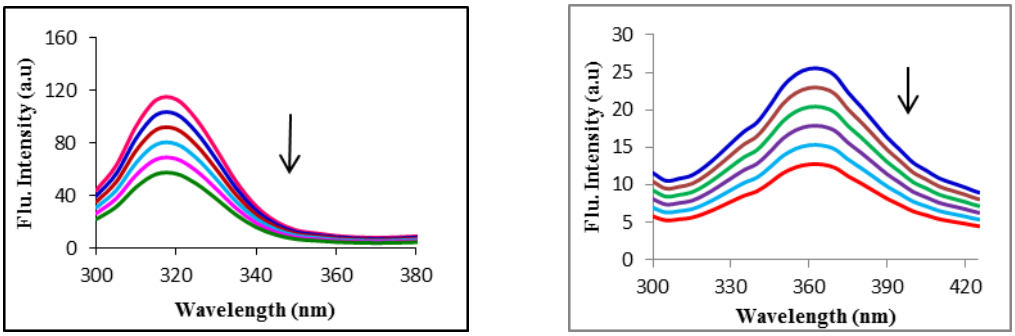

Fig.12 Synchronous Fluorescence Spectra for BHb with Cur - NS a) Δλ = 15 nm and b) Δλ = 60 nm

3.7. The Energy Transfer

Forster resonance energy transfer (FRET) is a process that allows two light-sensitive molecules to exchange energy [40]. A donor may send energy to an acceptor when in the electronic excited state. Equation [34] can be used to measure the utility of this energy transfer (E).

$$E = F/F_O = R^6_0/R^6_0+r^6_0 \quad (3)$$

The fluorescence intensity of BHb with and without the acceptor are denoted by F and F_0, respectively. When the energy transfer efficiency is 50%, R_0 denotes the critical distance. The average distance between the donor and acceptor is denoted by r. The following equation [41] can be used to calculate R_0:

$$R^6_0 = 8.8 \times 10^{-25} k^2 N^{-4} \Phi J(\lambda) \qquad (4)$$

Where K^2 is the dipole's spatial orientation factor with $K^2=2/3$ for random orientation in the solution, Φ represent the fluorescence quantum yield of the donor without acceptor, which is 0.062 for BHb, N is the medium's average refractive index, which in this case is 1.36 [42], and J(λ) is the spectral overlap intrinsic between the emission and absorption spectra, which can be determined by the equation [41].

$$J(\lambda) = \frac{\Sigma F(\lambda)\, \varepsilon(\lambda)\lambda^4 \Delta\lambda}{\Sigma F(\lambda)\Delta\lambda} \qquad (5)$$

Where F(λ) represents the donor's normalised fluorescence strength at wavelength (λ) and ε(λ) denotes the acceptor's extinction coefficient. J(λ) was calculated using the overlapped component of BHb's emission spectrum and Cur-NS's absorption spectrum, as seen in Fig.13, and it was 10.04 x 10^{-15} cm^3 M^{-1}. Furthermore, the E, R_0, and r values were 46%, 2.19 nm and 2.23 nm, respectively. Since the distance between BHb and Cur-NS was beneath 8nm [41], the energy transfer from BHb to Cur-NS exist with an immense probability.

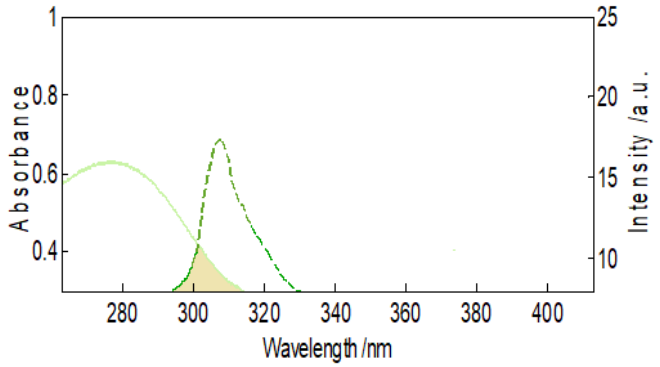

Fig.13 The overlap of UV absorption spectra of Cur – NS (solid line) with the fluorescence emission spectra of BHb (dotted line)

3.8 FTIR and FT-Raman Studies

For a long time, FTIR spectroscopy has shown the ability to detect confirmational variations at the inferior complex level in proteins. The amide band of a protein is composed predominantly of amide-I (1600-1700 cm^{-1}) and amide-II (1500-1600 cm^{-1}). The amide-II band, on the other hand, has a rather complex correlation, so the amide-I is often used for perceptible investigation of protein secondary structure elements. The amide-I band is generated by the C=O stretching vibration of the peptide backbone, which is dependent on the strength of the hydrogen bond and the interactions between the amide groups [43]. The FTIR spectra of BHb and BHb with Cur-NS are seen in Figs 14a and 14b. Pure BHb has an extreme band in the amide-I province that centres at 1652 cm^{-1}, showing that it is in a α-helix rich confirmation. The characteristics peak shifts 1652.3 cm^{-1} for Cur-NS–BHb complex. It's worth mentioning that the similarity in the nature of the two spectra meant that in the presence of Cur-NS, the basic features of the BHb secondary structure were retained [44].

The representation of bovine hemoglobin and Cur-NS was done using Raman spectroscopy in this study [45]. The FT-Raman spectra of bovine haemoglobin with Cur-NS are seen in Figs 15a and 15b.

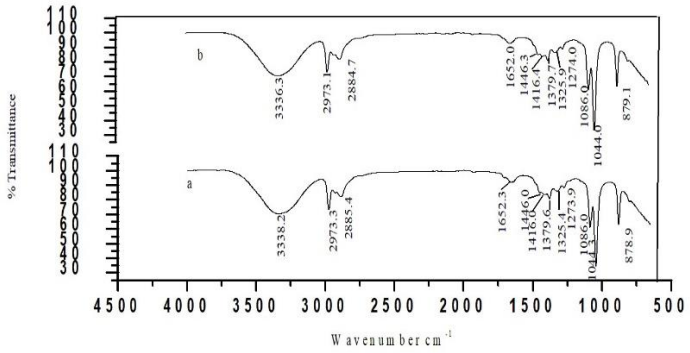

Fig.14 FTIR spectra of a) BHb b) BHb+ Cur-NS.

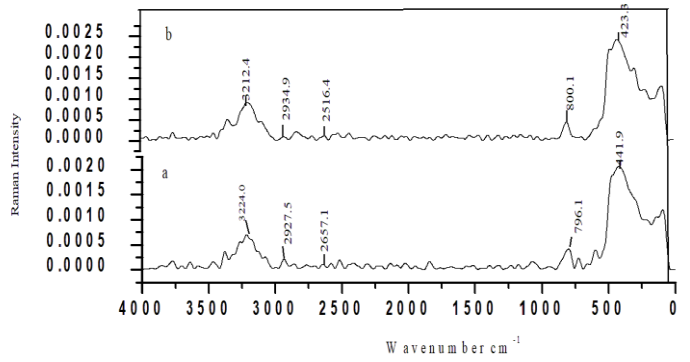

Fig.15 FT-Raman spectra of a) BHb b) BHb+ Cur-NS.

3.9. Molecular docking

Molecular docking simulations were used to further explore the binding sites of the Cur-NS-BHb complex, and the elite docking energy finding is shown in Fig.16. At the α1β2 interface of BHb, Cur-NS enters the hydrophobic pock. The results show that hydrophobic force dominates the interaction between BHb and Cur-NS. The results are similar to the experimental procedure obtained. The binding sites were acquired as α1-137Thr, α1-138Ser, α1-140Tyr, α1-141Arg, α2-127Lyz, β2-36Pro, β2-37Trp. Residues α-140Tyr and β-37Trp are located near Cur-NS, which provides a strong structural foundation for effective BHb emission quenching in the presence of Cur-NS. It is also consistence with the synchronous fluorescence results.

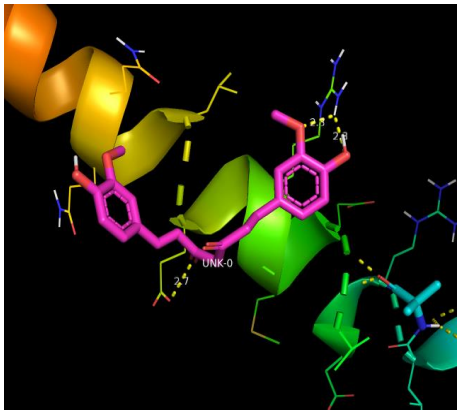

Fig.16 Docking image of BHb with Cur-NS

3.10 Antibacterial activity

The antibacterial activity of Cur-NS and BHb was tested using the agar well diffusion method (Fig. 17). As seen on the plates, the sample had reacted to antibacterial activity. For antibacterial function testing, Escherichia coli, Salmonella species, and Vibrio Cholerae (Gram-negative) and Staphylococcus species, (Gram-positive) bacterial models were used. Cur-NS-BHb is an important antibacterial substance.

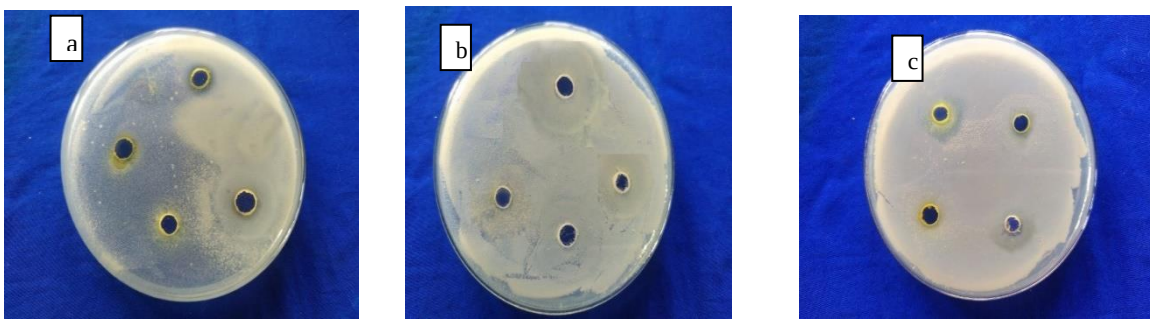

Fig .17 Antibacterial activity of a) Cur-NS b) BHb c) BHb with Cur-NS

4. Conclusions

In this analysis the relationship between Cur NS and BHb has been informative. The results reveal that Cur-NS could bind to BHb using a static quenching process. Cur-NS altered the conditions of Trp and Tyr residues, according to the effects of synchronous fluorescence spectra. A molecular docking analysis confirmed these findings. Cur-NS binding experiments with BHb not only revealed toxicological significance, but also revealed knowledge concerning BHb interactions with food colourant.

References

1. Patra, D., & Barakat, C. (2011). Synchronous fluorescence spectroscopic study of solvatochromic curcumin dye. Spectrochimica Acta Part A: Molecular and Biomolecular Spectroscopy, 79(5), 1034-1041.

2. Barik, A., Priyadarsini, K. I., & Mohan, H. (2003). Photophysical Studies on Binding of Curcumin to Bovine Serum Albumin¶. Photochemistry and photobiology, 77(6), 597-603.

3. Wang, F., Wu, X., Wang, F., Liu, S., Jia, Z., & Yang, J. (2006). The sensitive fluorimetric method for the determination of curcumin using the enhancement of mixed micelle. Journal of Fluorescence, 16(1), 53-59.

4. Barik, A., Mishra, B., Kunwar, A., & Priyadarsini, K. I. (2007). Interaction of curcumin with human serum albumin: Thermodynamic properties, fluorescence energy transfer and denaturation effects. Chemical Physics Letters, 436(1-3), 239-243.

5. Clifford, N. W., Iyer, K. S., & Raston, C. L. (2008). Encapsulation and controlled release of nutraceuticals using mesoporous silica capsules. Journal of Materials Chemistry, 18(2), 162-165.

6. Bisht, S., Feldmann, G., Soni, S., Ravi, R., Karikar, C., Maitra, A., & Maitra, A. (2007). Polymeric nanoparticle-encapsulated curcumin (" nanocurcumin"): a novel strategy for human cancer therapy. Journal of nanobiotechnology, 5(1), 1-18.

7. Leung, M. H., Colangelo, H., & Kee, T. W. (2008). Encapsulation of curcumin in cationic micelles suppresses alkaline hydrolysis. Langmuir, 24(11), 5672-5675.

8. Rankin, M. A., & Wagner, B. D. (2004). Fluorescence enhancement of curcumin upon inclusion into cucurbituril. Supramolecular Chemistry, 16(7), 513-519.

9. Baglole, K. N., Boland, P. G., & Wagner, B. D. (2005). Fluorescence enhancement of curcumin upon inclusion into parent and modified cyclodextrins. Journal of Photochemistry and Photobiology A: Chemistry, 173(3), 230-237.

10. Jovanovic, S. V., Boone, C. W., Steenken, S., Trinoga, M., & Kaskey, R. B. (2001). How curcumin works preferentially with water soluble antioxidants. Journal of the American Chemical Society, 123(13), 3064-3068.

11. Vemula, P. K., Li, J., & John, G. (2006). Enzyme catalysis: tool to make and break amygdalin hydrogelators from renewable resources: a delivery model for hydrophobic drugs. Journal of the American Chemical Society, 128(27), 8932-8938.

12. Jovanovic, S. V., Steenken, S., Boone, C. W., & Simic, M. G. (1999). H-atom transfer is a preferred antioxidant mechanism of curcumin. Journal of the American Chemical Society, 121(41), 9677-9681.

13. Wang, Y., Wang, K. M., Shen, G. L., & Yu, R. Q. (1997). A selective optical chemical sensor for o-nitrophenol based on fluorescence quenching of curcumin. Talanta, 44(7), 1319-1327.

14. Chignell, C. F., Bilskj, P., Reszka, K. J., Motten, A. G., Sik, R. H., & Dahl, T. A. (1994). Spectral and photochemical properties of curcumin. Photochemistry and photobiology, 59(3), 295-302.

15. Govindarajan, V. S., & Stahl, W. H. (1980). Turmeric—chemistry, technology, and quality. Critical Reviews in Food Science & Nutrition, 12(3), 199-301.

16. Aggarwal, B. B., Kumar, A., & Bharti, A. C. (2003). Anticancer potential of curcumin: preclinical and clinical studies. Anticancer research, 23(1/A), 363-398.

17. Chauhan, D. P. (2002). Chemotherapeutic potential of curcumin for colorectal cancer. Current pharmaceutical design, 8(19), 1695-1706.

18. Sułkowska, A. (2002). Interaction of drugs with bovine and human serum albumin. Journal of molecular structure, 614(1-3), 227-232.

19. Bhavsar, M.D., & Amiji, M.M. (2007). Gastrointestinal distribution and in vivo gene transfection studies with nanoparticles-in microsphere oral system (NiMOS). J. Control Release, 119, 339–348.

20. Sun, W., Zhang, N., & Li, X. (2012). Release mechanism studies on TFu nanoparticles-in-microparticles system. Colloids Surf B Biointerfaces, 95, 115–120.

21. Morris, G.M., Goodsell, D.S., Halliday, R.S., Huey, R., Hart, W.E., Belew, R.K., & Olson, A.J. (1998). Automated docking using a Lamarckian genetic algorithm and an empirical binding free energy function. J. Comput. Chem., 19, 1639–1662.

22. Galeano, E., & Martinez A. (2007). Antimicrobial activity of marine sponges from Uraba Gulf, Colombian caribean region. J. Med Mycol., 17, 21-24.

23. Manmode, A.S., Sakarkar, D., & Mahajan, N., (2009). Nanoparticles Tremendous Therapeutic Potential: a Review. Int. J.Pharm. Tech. Res., 1(4), 1020-1027.

24. Pan, C.J., Tang, J.J., Weng, Y.J., Wang, J., & Huang, N. (2006). Preparation, characterization and anticoagulation of curcumin-eluting controlled biodegradable coating stents. J. Control. Release, 116, 42–49.

25. Matsui, M., Nakahara, A., Takatsu, A., Kato, K., & Matsuda, N. (2008). International Journal of Chemical and Biomolecular Engineering, 1, 72–75.

26. Nassar, A. E. F., Rusling, J. F., & Nakashima, N. (1996). Electron transfer between electrodes and heme proteins in protein− DNA films. Journal of the American Chemical Society, 118(12), 3043-3044.

27. He, W., Li, Y., Si, H., Dong, Y., Sheng, F., Yao, X., & Hu, Z. (2006). Molecular modeling and spectroscopic studies on the binding of guaiacol to human serum albumin. Journal of Photochemistry and Photobiology A: Chemistry, 182(2), 158-167.

28. Zolghadri, S., Saboury, A. A., Amin, E., & Moosavi-Movahedi, A. A. (2010). A spectroscopic study on the interaction between ferric oxide nanoparticles and human hemoglobin. Journal of the Iranian Chemical Society, 7(2), S145-S153.

29. Zhou, J., Wu, X., Gu, X., Zhou, L., Song, K., Wei, S., Feng, Y., & Shen, J. (2009). Spectroscopic studies on the interaction of hypocrellin A and hemoglobin. Spectrochim. Acta A, 72, 151–155.

30. Li, Z., Li, Z.G., Yang, L.L., Xie, Y.Z., Shi, J., Wang, R.Y., & Chang, J.B. (2015). Investigation of the binding between pepsin and nucleoside analogs by spectroscopy and molecular simulation. J. Fluoresc., 25, 451–463.

31. Lakowicz, J.R. (1999). Principles of fluorescence spectroscopy. Second ed. Plenum Press, New York, 237.

32. Lakowicz, J.R. (2006). Principles of Fluorescence Spectroscopy. third ed. Springer Science + Business Media, New York, 63–606

33. Peng, W., Ding, F., Peng, Y.-K., & Sun, Y., (2014). Molecular recognition of malachite green by hemoglobin and their specific interactions: insights from in silico docking and molecular spectroscopy. Mol. BioSyst., 10, 138–148.

34. Zhang, Y. Z., Zhou, B., Zhang, X. P., Huang, P., Li, C. H., & Liu, Y. (2009). Interaction of malachite green with bovine serum albumin: determination of the binding mechanism and binding site by spectroscopic methods. Journal of Hazardous Materials, 163(2-3), 1345-1352.

35. Zhang, G., Ma, Y., Wang, L., Zhang, Y., & Zhou, J. (2012). Multispectroscopic studies on the interaction of maltol, a food additive, with bovine serum albumin. Food chemistry, 133(2), 264-270.

36. Lloyd, J.B.F. (1971). Multicomponent analysis by synchronous luminescence spectrometry. Nature, 231, 64–65.

37. Miller, J.N. (1979). Recent advances in molecular luminescence analysis. Proc. Anal. Div. Chem. Soc., 16 (7), 203–208.

38. Wang, Y. Q., & Zhang, H. M. (2012). Investigations on the binding of human hemoglobin with orange I and orange II. Journal of Photochemistry and Photobiology B: Biology, 113, 14-21.

39. Wang, Y. Q., Zhang, H. M., Zhou, Q. H., & Xu, H. L. (2009). A study of the binding of colloidal Fe3O4 with bovine hemoglobin using optical spectroscopy. Colloids and Surfaces A: Physicochemical and Engineering Aspects, 337(1-3), 102-108.

40. Shi, J.H., Chen, J., Jing, W., Zhu, Y.Y., & Qi, W. (2015). Spectrochim. Acta A Mol. Biomol. Spectrosc., 149, 630–637.

41. Wang, Q., Huang, C.R., Jiang, M., Zhu, Y.Y., Wang J., Chen, J., & Shi, J.H. (2016). Spectrochim. Acta A Mol. Biomol. Spectrosc., 156, 155–163.

42. Haouz, A., El, M.S., Zentz, C., Merola, F., & Alpert, B. (1999). Eur. J. Biochem., 264, 250–257.

43. Mahato, M., Pal, P., Kamilya, T., Sarkar, R., & Talapatra, G.B. (2010). J. Phys. Chem. B, 114, 495–502.

44. Tang, J., Yang, C., Zhou, L., Ma, F., Liu, S., Wei, S. & Zhou, Y. (2012). Studies on the binding behavior of prodigiosin with bovine hemoglobin by multi-spectroscopic techniques. Spectrochimica Acta Part A: Molecular and Biomolecular Spectroscopy, 96, 461-467.

45. Frank, C.J. & Pelletier (Ed.), M.J. (1999). Analytical Application of Raman Spectroscopy. Blackwell Science, United Kingdom, 224-271.